#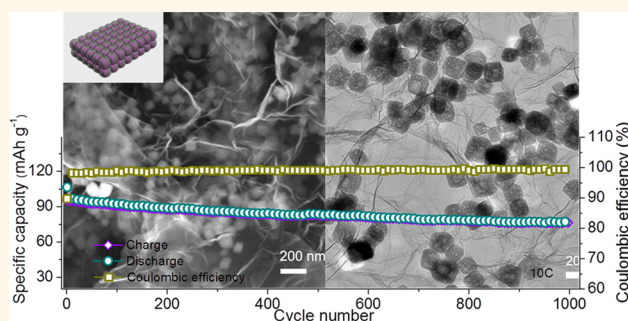 Synthesizing Porous NaTi$_2$(PO$_4$)$_3$ Nanoparticles Embedded in 3D Graphene Networks for High-Rate and Long Cycle-Life Sodium Electrodes

Chao Wu,[‡] Peter Kopold,[‡] Yuan-Li Ding,[‡] Peter A. van Aken,[‡] Joachim Maier,[‡] and Yan Yu[*,†,‡]

[†]Key Laboratory of Materials for Energy Conversion, Chinese Academy of Sciences, Department of Materials Science and Engineering, University of Science and Technology of China, Hefei 230026, Anhui, China and [‡]Max Planck Institute for Solid State Research, Heisenbergstraße 1, Stuttgart 70569, Germany

ABSTRACT Sodium ion batteries attract increasing attention for large-scale energy storage as a promising alternative to the lithium counterparts in view of low cost and abundant sodium source. However, the large ion radius of Na brings about a series of challenging thermodynamic and kinetic difficulties to the electrodes for sodium-storage, including low reversible capacity and low ion transport, as well as large volume change. To mitigate or even overcome the kinetic problems, we develop a self-assembly route to a novel architecture consisting of nanosized porous NASICON-type NaTi$_2$(PO$_4$)$_3$ particles

embedded in microsized 3D graphene network. Such architecture synergistically combines the advantages of a 3D graphene network and of 0D porous nanoparticles. It greatly increases the electron/ion transport kinetics and assures the electrode structure integrity, leading to attractive electrochemical performance as reflected by a high rate-capability (112 mAh g^{-1} at 1C, 105 mAh g^{-1} at 5C, 96 mAh g^{-1} at 10C, 67 mAh g^{-1} at 50C), a long cycle-life (capacity retention of 80% after 1000 cycles at 10C), and a high initial Coulombic efficiency (>79%). This nanostructure design provides a promising pathway for developing high performance NASICON-type materials for sodium storage.

KEYWORDS: NaTi$_2$(PO$_4$)$_3$ · 3D graphene-network · mesoporous nanoparticles · ultrafast sodium storage · long-cycle life

L ithium-ion batteries (LIBs) have been extensively investigated in the past few decades and widely used as renewable power source for applications in various portable electronics.[1] However, the increasing demands for their applications in grid-scale energy storage such as electric vehicles and smart grids raise considerations concerning the high cost and the limited resources of lithium.[2] As alternative, sodium ion batteries (SIBs) are considered as good candidates for large-scale energy storage applications owing to their low-cost and earth-abundant sources.[3,4]

Recently,[5−9] NASICON-type NaTi$_2$(PO$_4$)$_3$ (NTP) has been considered as attractive SIB electrode because of high theoretical capacity of 133 mAh g^{-1}, high Na$^+$ conductivity, and pronounced thermal stability. Owing to the moderate voltage range, it can, depending to the counter electrodes,

be used as anode and cathode. In previous studies,[10−12] it was proposed as sodium anode, for which there is a great demand. As SIB anodes, the commonly used commercial graphite electrodes show very low reversible capacities as the Na ion (radium 0.95 Å) is about 55% larger than the Li ion (0.6 Å).[13] Great research efforts[14,15] have been made to develop suitable anode materials with high storage capacity, high rate-capability, and remarkable cycle-stability. Currently, there have been a few well-working anode materials that have been identified for SIBs, including hard carbon,[16] Na$_2$Ti$_3$O$_7$,[17] P/carbon,[18] alloy (Sn and Sb),[19−22] Sn$_4$P$_3$,[23] and SnS$_2$.[24] However, the aggravated ion transport and the more severe volume change of SIBs cause inferior electrochemical performances of these anode materials when compared to LIBs in terms of low initial
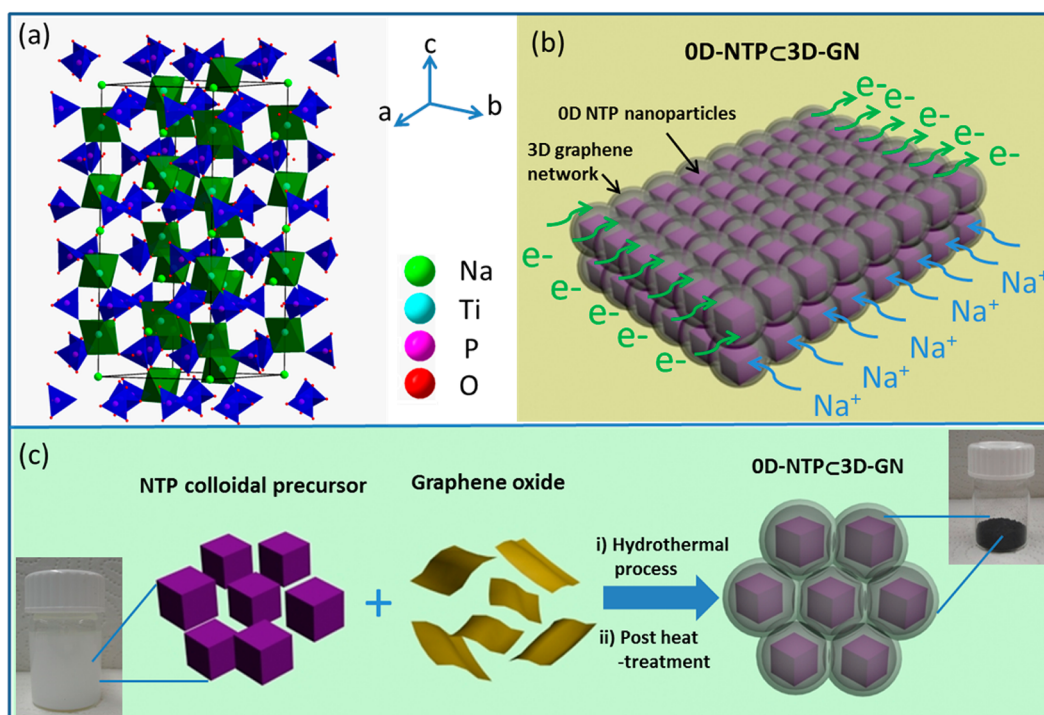
Figure 1. (a) Crystal structure of the NTP phase. (b) Schematic illustration of 0D-NTP⊂3D-GN, showing that 0D porous NTP nanoparticles are embedded in 3D graphene network. (c) Schematic synthesis of 0D-NTP⊂3D-GN, including the two steps of hydrothermal process and postheat treatment.

Coulombic efficiency (CE), low rate-capability and poor cycle-stability.

As shown in Figure 1a, NTP exhibits a three-dimensional (3D) framework structure[5−7] with TiO_6 octahedra and PO_4 tetrahedra sharing all their corner oxygen atoms, giving rise to roomy interstices.[5] Thus, NTP has a high Na^+ conductivity which is a decisive advantage for electrochemical storage kinetics. In addition, NASICON-type NTP is well-known as an intercalation material with low volume change during Na insertion and extraction for room-temperature SIBs. The previous studies indicate that NTP has a relatively high voltage plateau at *ca.* 2.1 V *vs* Na^+/Na.[6] Although the relatively high redox potential of NTP sacrifices energy density to some extent when compared to other anodes (*e.g.*, hard carbon), it is the same point that renders it intrinsically much safer during fast charging and also reduces the possibility of forming a solid electrolyte interface (SEI).[16,25] However, similar to other NASICON-type materials[26,27] (*e.g.*, $Na_3V_2(PO_4)_3$), the practical applications of NTP are severely hindered by the low capacity release and the poor cycle stability owing to its low electronic conductivity. In principle, several approaches[26] have been proposed to increase the transport kinetics of NASICON-type materials. One is to vary the composition of these electroactive materials by doping to improve their transport properties. Another is to provide an effective conductive network by combining NTP with electrically conductive materials (*e.g.*, carbon). The

third is to reduce the size of electroactive materials to shorten the electron/ion transport path. Currently, the synthesis of NTP is mainly relying on a solid-state reaction approach because of its multicomponent and complex crystal structure;[6,11,12,28,29] it is difficult to control morphology and size of crystalline NTP, and only NTP micrometer-sized particles and nanoaggregates are currently available. Even upon coating these NTP particles with carbon, they still show an unsatisfied electrochemical performance in terms of rate-capability and cycle-lifetime as anodes for sodium storage.[9,10,12,29,30]

Herein, we realize for the first time an architecture that comprises embedded porous NTP nanoparticles in a 3D graphene network (0D-NTP⊂3D-GN). As shown Figure 1b, this novel structure provides multiple advantages: (i) the porous structure and the nanosize of the NTP particles provide much more active sites and shorten the solid-state ion/electron transport path in the crystal, respectively; (ii) the 3D interconnected graphene network counteracts self-aggregation of NTP particles assuring structural integrity and facilitating electron transfer on cycling. As a result, the obtained NTP⊂GN shows excellent electrochemical performances in terms of reversible capacity, rate-capability, cycle-stability as well as Coulombic efficiency: the reversible capacity reaches 100 mAh g^{-1} at up to 5C (polarization being very small); the anodes deliver 67 mAh g^{-1} at a rate as high as 50C (6.6 A g^{-1}); the reversible capacity can retain
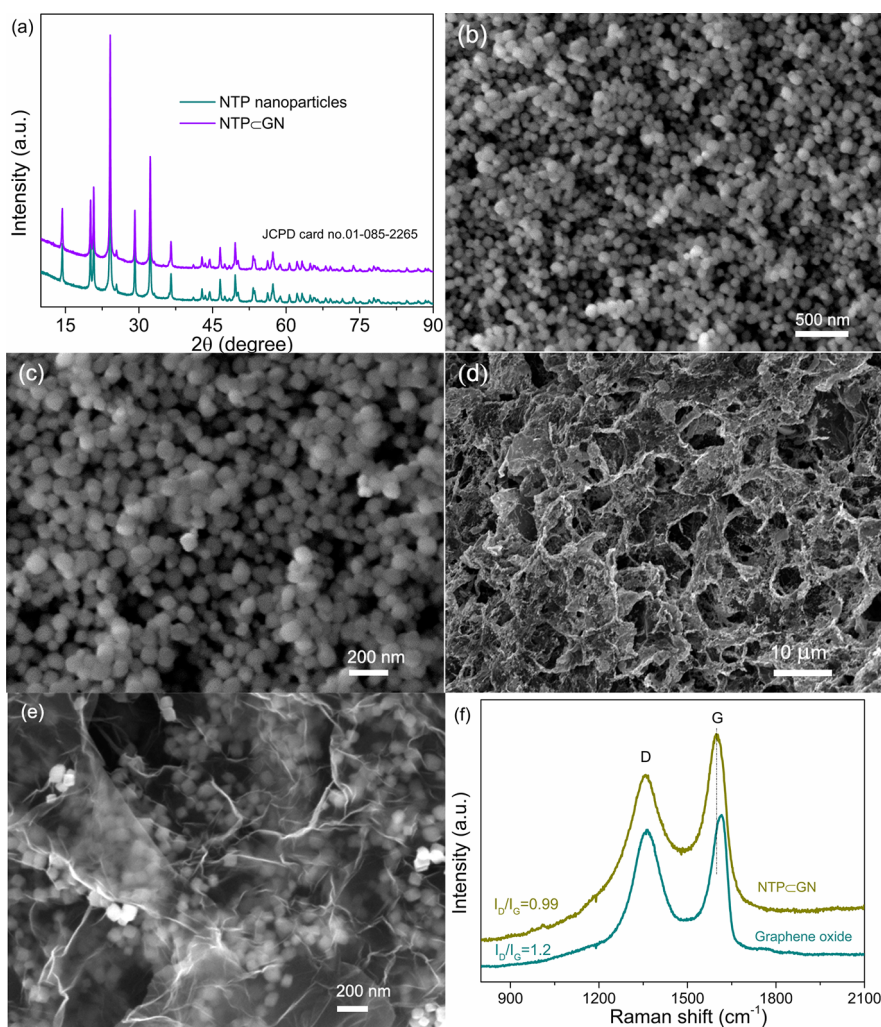
Figure 2. Crystal structure and morphology characterization: (a) XRD patterns of the NTP nanoparticles and NTP⊂GN; SEM images of the (b and c) NTP nanoparticles and (d and e) NTP⊂GN; (f) Raman spectra of graphene oxide (GO) and NTP⊂GN. Notably, the NTP particles undergo the postheat treatment (annealing at 600 °C for 2 h in Ar).

80% after 1000 cycles at 10C; the CE value is as high as 79% at the initial cycle and remains 98% after 200 cycles at 1C.

RESULTS AND DISCUSSION

Figure 1c displays the overall synthesis process of the NTP⊂GN architecture, which is different from the conventional solid-state method. In the reported solid-state approach, sodium salt, titanium oxide, and phosphate salt were mixed to form a precursor. After annealing the precursor at high temperature (800 °C), only microsized NTP particles or nanosized NTP aggregates were obtained. Post carbon-coating treatment usually made this coating incomplete and inhomogeneous. In this study, porous NTP nanoparticles are homogeneously encapsulated in a 3D conductive graphene network by a self-assembly route. Graphene exhibits high electrical conductivity, high surface area, and excellent chemical stability, and thus is applied to build a 3D conductive network with replacing the traditional amorphous carbon-coating. For the

synthesis of NTP⊂GN, we first prepare a highly stable NTP colloidal precursor which is the key to obtain NTP⊂GN. These NTP colloidal nanoparticles do not sediment at the bottom even if the solution was stored for 2 days (Figure 1c). Next, the NTP colloidal precursor was assembled with graphene oxide (GO) by a hydrothermal process and post heat-treatment, resulting in the desired NTP⊂GN (the detained procedure description is given in the Methods section).

Figure 2a show the X-ray diffraction (XRD) patterns of NTP nanoparticles and NTP⊂GN. Notably, the NTP particles are available by the same post heat-treatment of the NTP precursor as NTP⊂GN. All the diffraction peaks of NTP nanoparticles and NTP⊂GN are indexed to $NaTi_2(PO_4)_3$ (JCPDS no. 01-085-2265). For NTP⊂GN, no extra graphite phase ($2\theta = 26°$, corresponding to the (002) plane of graphite) is observed, indicating that the NTP nanoparticles can prevent graphene from aggregating into graphite sheets during the synthesis process. Moreover, according to Rietveld refinement (Supporting Information Figure S1), the NTP crystalline
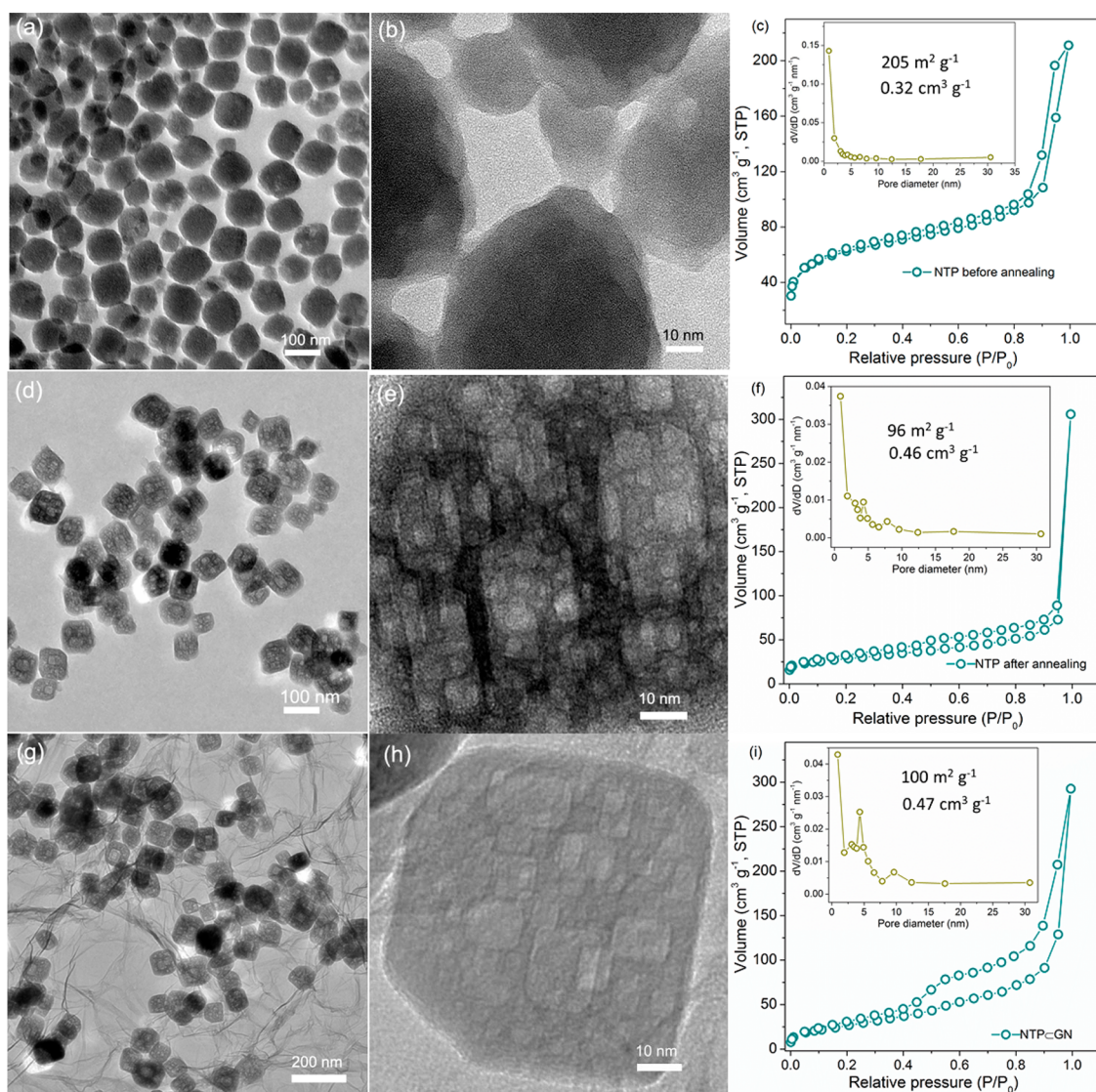
Figure 3. Nanostructure and porosity characterization: (a) TEM and (b) HRTEM images as well as (c) nitrogen adsorption/desorption isotherms of the NTP precursor without annealing treatment; (d) TEM and (e) HRTEM images as well as (f) nitrogen adsorption/desorption isotherms of the NTP nanoparticles after annealing at 600 °C for 2 h in Ar; (g) TEM and (h) HRTEM images and (i) nitrogen adsorption/desorption isotherms of NTP⊂GN.

shows the NASICON-type structure with space group $R\bar{3}c$ (no. 167) and lattice parameters a = 8.4764(26) Å and c = 21.7721(40) Å. The morphology and microstructure of NTP particles and NTP⊂GN are investigated by scanning electron microscopy (SEM). As shown in Figure 2b,c, many cube-like nanoparticles are detected in a size range from about 50 to 100 nm. For NTP⊂GN, almost all NTP nanoparticles are wrapped by graphene sheets which are connected into the desired 3D conductive network (Figure 2d,e). The existence of a graphene network is also confirmed by Raman spectra which reveal pronounced D and G bands at around 1358 and 1599 cm^{-1}, respectively (Figure 2f). Compared to GO, the G band shifts to low frequency, indicating a significant removal of oxygen-containing groups on the GO surface during the hydrothermal and post heat-treatment process.[31]

Furthermore, the NTP⊂GN sample shows a lower peak intensity of the D and G bands (I_D/I_G = 0.99) when compared to the GO precursor (I_D/I_G = 1.2) indicating the electronic conjugation after reduction,[32] and hence high electronic conductivity, resulting in remarkable rate-performance of NTP⊂GN.

To examine the detailed nanostructure of the as-prepared materials, we further perform transmission electron microscopy (TEM) and nitrogen isothermal adsorption technique. TEM images (Figure 3) show many individual cube-like NTP nanoparticles with sizes around 50−100 nm, consistent with the SEM result. The size of the NTP particles is much less than that of previously reported NTP microparticles obtained by a solid-state approach.[9] Notably, these NTP nanoparticles show porous nanostructure, and mesopores are clearly observed in the high-resolution TEM (HRTEM)
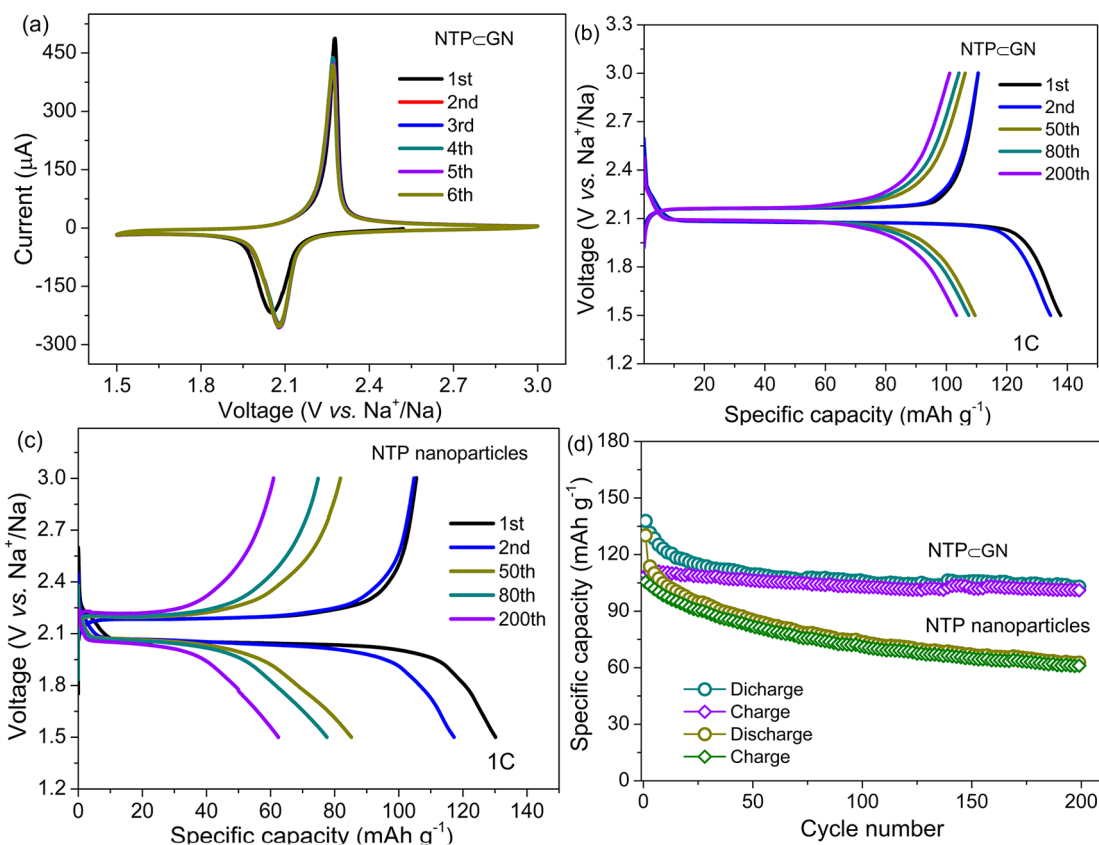
Figure 4. (a) Cyclic voltammetry (CV) curves of the NTP⊂GN electrode for the initial 6 cycles at a scanning rate of 0.2 mV s^{-1}. The discharge−charge profiles of the (b) NTP⊂GN and (c) NTP particle electrodes at 1C. (d) Cycling performance of the NTP⊂GN and NTP particle electrodes at 1C (assumed 1C = 133 mA g^{-1}). Note that all the capacity values for the NTP⊂GN electrodes are calculated based on the mass of NTP, which is 65% of the whole electrodes including NTP, graphene, carbon black, and PVDF.

image (Figure 3e). Such cube-like nanoparticles with mesoporous nanostructure have rarely been reported. However, before postheat treatment (annealing at 600 °C), the NTP precursor, although of similar morphology and size to that after annealing, shows no mesoporous nanostructure in the HRTEM image (Figure 3b). Obviously, the annealing process is responsible for the formation of mesopores, but interestingly does not increase the size of the nanoparticles. The TEM images of NTP⊂GN reveal that the NTP nanoparticles are also embedded in the 3D graphene network, and that these wrapped particles have a similar mesoporous nanostructure, which is beneficial for sodium-ion transport. HRTEM images of the NTP particles and NTP⊂GN further reveal clear lattice fringes with *d*-spacings of 0.61 and 0.36 nm, corresponding to the (012) and (113) planes of NASICON-type phase, and hence a high degree of crystallinity (Supporting Information Figure S2). It should be noted that no crystallinity was observed in the HRTEM horizon for NTP colloid particles without annealing treatment. All these samples display typical type IV isothermal adsorption−desorption curves, as shown in Figure 3. Before annealing, the NTP nanoparticles show a specific surface area of 205 m^2 g^{-1} with a total pore volume of 0.32 cm^3 g^{-1},

and the Barrett−Joyner−Halenda (BJH) pore-size distribution curve shows pore sizes in the range of 1−2 nm (micropores). After annealing, the surface area of the NTP sample decreases to 96 m^2 g^{-1} and the corresponding total pore volume increases to 0.46 cm^3 g^{-1} with a pore size range from 1 to 10 nm, indicating that the mesopores originate from the transformation of micropores, possibly caused by the high-temperature-driven crystallization of amorphous parts. NTP⊂GN shows a surface area of 100 m^2 g^{-1} and a total pore volume of 0.47 cm^3 g^{-1}, and the corresponding pore size distribution is in the range of 1−10 nm, which is close to that of the NTP particles after annealing.

The electrochemical behaviors of the NTP nanoparticles and NTP⊂GN were evaluated using coin-type cells with sodium metal as counter electrode and with 1 M NaClO$_4$ in ethylene carbonate (EC)−diethyl carbonate (DEC) as electrolyte. Figure 4a displays the cyclic voltammetry (CV) curves of the NTP⊂GN electrode in the range from 1.5 to 3 V for the initial six cycles, recorded at a scan rate of 0.2 mV s^{-1}. In the first cycle, a single reduction peak is located at ∼2.05 V, and another peak corresponding to oxidation appears at ∼2.28 V. This pair of well-defined sharp redox peaks

correspond to the redox reaction of Ti^{4+}/Ti^{3+} for NTP⊂GN, as follows:[10]

$$NaTi_2(PO_4)_3 + 2Na^+ + 2e^- \leftrightarrow Na_3Ti_2(PO_4)_3$$
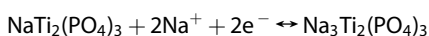
From the second cycle, the reduction peaks are shifted to ∼2.08 V and the oxidation peaks are still at around 2.28 V. The initial tiny voltage increase is mainly ascribed to the stress/strain change, consistent with previous reported NASICON-type materials.[33] The redox polarization is about 0.2 V, lower than that of the NTP nanoparticle electrode (Supporting Information Figure S3) and that of the reported NTP materials in aqueous and nonaqueous electrolytes.[9,29] Furthermore, CV curves overlap after the first cycles, indicating remarkable reversibility.

NTP⊂GN shows excellent electrochemical performances in terms of sodium storage. Figure 4b displays the representative galvanostatic charge/discharge profiles of NTP⊂GN at 1C within a cutoff voltage between 1.5 and 3 V. Notably, 1C means that the full capacity will be discharged or charged in 1 h, corresponding to a current density of 133 mA g^{-1}. The first discharge and charge capacities are 138 and 109 mA g^{-1}, respectively, corresponding to a CE of 79%, much higher than that of hard carbon[25] and metal alloy[20] because of its relatively high sodium-storage voltage platform. Note that all the capacity values for the NTP⊂GN electrodes are calculated based on the mass of NTP. Considering that the loading of graphene in NTP⊂GN is about 18% by weight, NTP is 65% of the whole electrode including NTP, graphene, carbon black, and polyvinylidene fluoride (PVDF). Supporting Information Figure S4 shows the discharge−charge profiles for the graphene electrode at 133 mA g^{-1}, the first and second discharge capacities 30 and 7 mAh g^{-1}, while the corresponding charge capacities are 0.61 and 0.57 mAh g^{-1}, respectively. Thus, the capacity contribution from graphene for the NTP⊂GN electrode is almost neglected for sodium storage. All the profiles of NTP⊂GN show a well-defined, flat, and symmetric discharge and charge plateaus, which is similar to rather LiFePO$_4$ and Na$_3$V$_2$(PO$_4$)$_3$ based on phase transition. The first discharge plateau is about 2.08 V, and the corresponding charge plateau is around 2.17 V, giving rise to a very small discharge−charge polarization of only 90 mV at 1C. Importantly, the small polarization is invariant with increasing cycling (Figure 4b), which is different from that of microsized carbon-coated NTP where the polarization is gradually increased with cycling.[8] The confinement of NTP in a 3D graphene-network is crucial for the small and stable polarization. For comparison, the porous NTP particles mixed with carbon black (super-P) are used as anodes for sodium-storage (super P instead of graphene-network). Figure 4c shows the display of the discharge−charge profiles for the NTP nanoparticles at 1C. Although they show a high CE value (81%) as well, the discharge−charge

polarization is around 155 mV, higher than that of NTP⊂GN. Small polarization for NTP⊂GN was attributed to the high ionic/electron conductivity and less severe solvation in the liquid, which is consistent with previously reported Na$_3$V$_2$(PO$_4$)$_3$ coated by double carbon shell.[26]

The cycle-stability of NTP⊂GN is outstanding as well, as demonstrated in Figure 4d. The reversible capacity is as high as 101 mAh g^{-1} after 200 cycles at 1C, corresponding to 93% capacity retention. In addition, the CE value remains 98% after 200 cycles. By contrast, the NTP particles undergo a rapid capacity fading. After 200 cycles, only a reversible capacity of 61 mAh g^{-1} is available, corresponding to 58% retention. Such poor cycle stability is attributed to the self-aggregation of NTP nanoparticles on cycling, leading to lose electrical contact with super-P and the current collector. For NTP⊂GN, graphene network plays an important role: not only does it prevent NTP particles from aggregating, but it also offers a well current-collecting network for electron transport. Supporting Information Figure S5 shows a SEM image of NTP⊂GN after 200 cycles, and the graphene network and cube-like NTP particles are still clearly identified. The crystalline structure of NTP⊂GN after cycling is also investigated by XRD technique, as shown in Supporting Information Figure S6. All the diffraction peaks are located at the same positions before and after cycling, indicating the robust structure of the NTP particles. This morphological and structure invariance is responsible for the excellent cycle stability.

Next, the NTP⊂GN anodes were further investigated by galvanostatic charge−discharge at various current rates from 0.5 to 50C, as shown in Figure 5a. Well-defined, flat and symmetric charge−discharge voltage plateaus are observed. In spite of perceptible polarization at the high current density (50C), the charge−discharge plateaus are still clearly distinguishable. The reversible capacities are 117, 112, 105, 96, 85 mAh g^{-1} at current rates of 0.5, 1, 5, 10, 20C, respectively (Figure 5b). Remarkably, even at a current rate as high as 50C, a reversible capacity of 67 mAh g^{-1} is available, indicating that the NTP⊂GN electrodes are able to get rapidly charged and discharged within several minute, thus delivering high energy and power density. This fast rate performance is comparable to that of super-capacitors. To our best knowledge, the high rate performance is unprecedented for the NTP anodes in nonaqueous SIBs[10,27] and higher than that in aqueous SIBs[12] (Figure 5c). Importantly, the specific capacity of NTP⊂GN electrode nearly recovers to the original value as the current rate returns to 1C after high-rate cycling, further demonstrating the structure integrity of electrodes. For the porous NTP particle anodes, they show a poor rate-performance, delivering no capacity at high current rate (>10C) because of lack of 3D conductive network in despite of having mesoporous
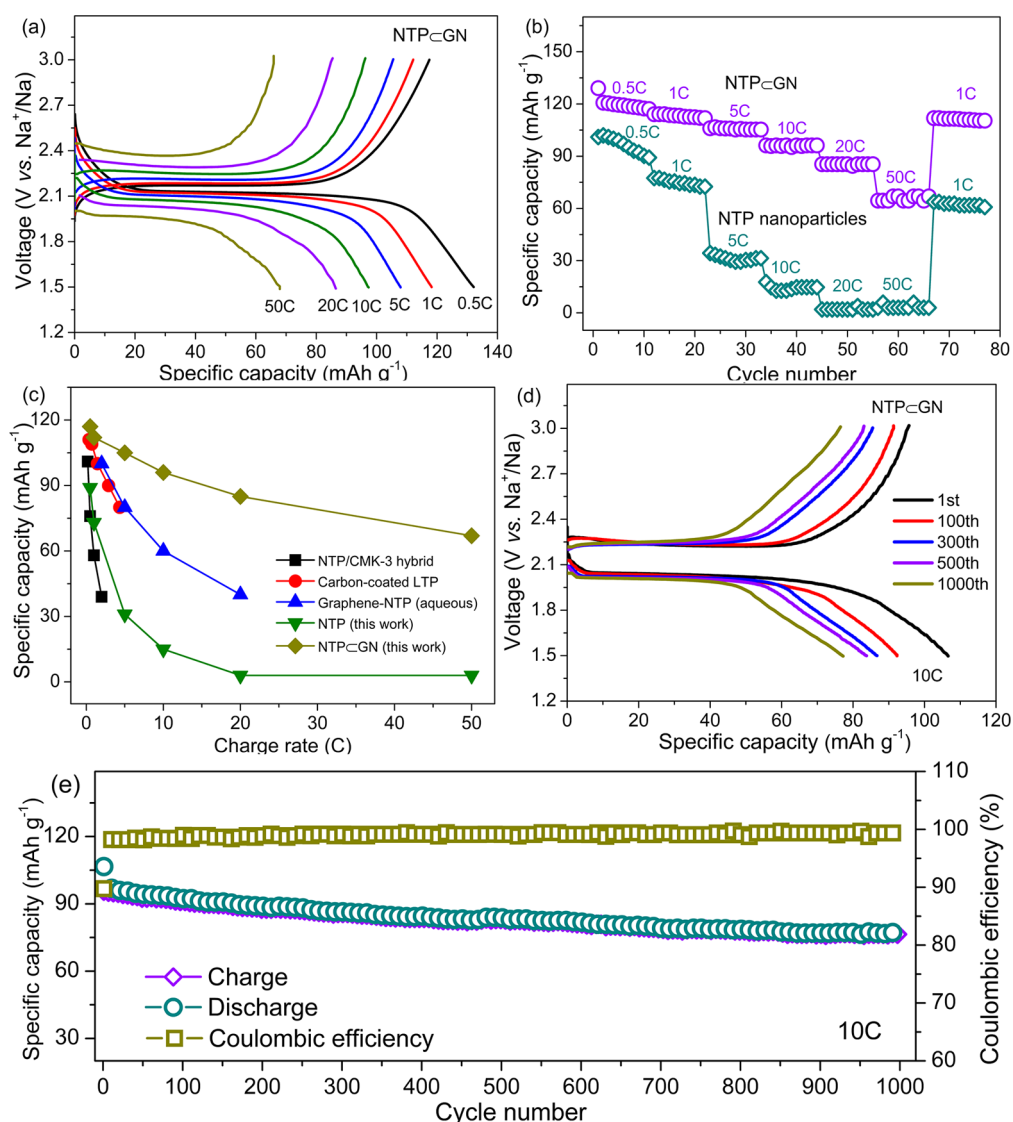
Figure 5. (a) Galvanostatic discharge–charge profiles of the NTP⊂GN electrode at various current rates. (b) Rate-performance and capacity retention ability of the NTP⊂GN and NTP particle electrodes. (c) Comparison of rate performance of the NTP⊂GN electrode to the recently reported results in literatures for NTP/CMK-3, carbon-coated LiTi₂(PO₄)₃(LTP), and graphene-NTP (corresponding refs, 10, 12, and 27). (d) The discharge–charge profiles and (e) long-cycling performance of the NTP⊂GN electrodes. Note that all the capacity values for the NTP⊂GN electrodes are calculated based on the mass of NTP, which is 65% of the whole electrodes including NTP, graphene, carbon black, and PVDF.

nanostructure. To reveal the reason for the enhanced electrochemical property of NTP⊂GN anode, the electrochemical impedance spectra were measured before cycling, as shown in Supporting Information Figure S7. The Nyquist plot for each of cells shows a depressed semicircle in the high frequency region, which may be associated with the charge transfer resistance (R_{ct}). This R_{ct} of NTP⊂GN anode is about 340 Ω, much less than that (748 Ω) of the NTP particle anode, indicating the beneficial role of the 3D graphene network for charge transfer kinetics.

To further demonstrate long cycle-life of the NTP⊂GN anode, we cycled the cell for 1000 cycles at a high current rate (10C), as shown in Figure 5d,e. The anodes show a reversible capacity as high as 96 mAh g⁻¹ at the first cycle, 85 mAh g⁻¹ at the

300th cycle, 83 mAh g⁻¹ at the 500th cycle. After 1000 cycles, the reversible capacity still reaches 77 mAh g⁻¹, corresponding to capacity retention of 80% for the first cycle (only 0.02% loss for per cycle). Such remarkable cycle stability for the NTP materials has not been reported before, significantly outperforming previously reported FeP[13] and metal alloy materials.[34,35] In addition, the CE value of NTP⊂GN anodes is 90% for the initial cycle, and it is as high as 99% for the 1000th cycle at 10C. This superior long-cycling and high-rate performance of the NTP⊂GN anode is attributed to the advantages of its unique morphology and the ionic properties. First, the 3D graphene-network encapsulation prevents the self-aggregation of NTP nanoparticles and the mesoporous nanostructure can mitigate the strain effects caused by the volume

change during repeated Na$^+$ insertion/extraction, which ensure the effective electrical contact between graphene and NTP particles on cycling, resulting in the attractive long cycle-life. Second, in spite of larger size for Na$^+$ ion compared to Li$^+$ ion, the Na$^+$ ion size is optimal for fast ion transport in the NASICON-type structure; simultaneously, the nanosize of NTP particles decrease the electron/ion transport path in the crystal and the mesoporous channels provide active sites for sodium intercalation. Furthermore, as the sodium ion is less strongly solvated in the liquid electrolyte than the lithium ion, the charge transfer between liquid and solid is facilitated. In addition, 3D graphene network provides continuous electron transport pathway for the NTP particles.

CONCLUSION

In summary, we propose and synthesize a novel architecture (NTP⊂GN) consisting of 0D (nanosized) porous NTP particles embedded in 3D (microsized) graphene network by a self-assembly process and postheat-treatment. Such novel architecture greatly facilitates the electron/ion transport kinetics of NTP⊂GN and guarantees the electrode structure integrity, leading to excellent electrochemical performance in terms of high rate-capability, long cycle-life and high initial CE value. The NTP⊂GN electrode is able to deliver a reversible capacity of 67 mAh g^{-1} at 50C, meaning that it can be charged and discharged within 1.2 min. This ultrafast performance of the NTP⊂GN electrodes is remarkable and exceeds, if used as anode, the performance of other SIB anodes (hard carbon and metal alloy), even comparable to that of supercapacitors. After 1000 cycles at 10C, it remains 80% retention of the initial charge capacity, outperforming the cycling-stability of the reported NTP and NTP/carbon anodes. This work clearly indicates that 0D-NTP⊂3D-GN with unique morphology and novel architecture has potential for the development of high-performance SIBs. Indeed, the NTP⊂GN electrodes display a relatively high voltage plateau (around 2.2 V *vs* Na$^+$/Na) as anodes. When NTP⊂GN electrode is used for a full cell, it requires to select some cathodes with high discharge potential to match and realize high power release (*e.g.*, Na$_3$V$_2$(PO$_4$)$_2$F$_3$ and Na$_4$Co$_{2.4}$Mn$_{0.3}$Ni$_{0.3}$(PO$_4$)$_2$P$_2$O$_7$).[36,37] It proposes a higher technological requirement on the cathode materials.

METHODS

Synthesis of NTP Nanopartciles. First, 2 mmol CH$_3$COONa and 2 mmol titanium(IV) butoxide were dissolved into 6 mL of phosphorous acid solution (85 wt %) and 40 mL of ethanol solvent, respectively. The above two solutions were mixed by magnetic stirring, and then transferred into Teflon vessel for solvent-thermal reaction. The autoclave volume is 100 mL, and it was purchased from the Parr Instrument company. After reaction for 3 h at 160 °C, the white wet products are available by centrifugation separation and washing by deionized water. The stable NTP colloidal precursor was obtained by redispersing the white product into water solution. The desired NTP nanoparticles were obtained by drying the wet product and following annealing treatment at 600 °C for 2 h in argon. The NTP precursor was available by direct drying the wet product.

Synthesis of NTP⊂GN. In a typical process, GO (100 mg) was first dispersed into 15 mL of aqueous solution. GO were prepared by the modified Hummers' method. Then, 10 mL of NTP colloidal solution (0.2 g solids) and 15 mL of GO dispersion were mixed by magnetic stirring and ultrasonic treatment. The resulting solution was transferred into hydrothermal autoclave with Teflon vessel. After reaction at 180 °C for 10 h, a monolithic gel-like product was obtained. The gel-like product was directly dried at 80 °C and then annealed in argon at 600 °C for 2 h to obtain the desired NTP⊂GN. The elemental analysis shows the loading of graphene is about 18 wt % for the NTP⊂GN sample.

Materials Characterization. The morphology and microstructure of the as-prepared samples were investigated by field-emission scanning electron microscopy (FE-SEM, Zeiss Gemini DSM 982) and transmission electron microscopy (TEM, JEOL 4000 FX, 400 kV). Nitrogen adsorption and desorption isotherms were measured with a Quanta Chrome Adsorption Instrument. The structures of the as-prepared samples were recorded by X-ray diffraction (XRD) (Philips) using Cu Kα radiation.

Electrochemical Measurement. The electrochemical performance of materials was carried out by the 2032-type coin-cell with a metallic sodium film as the counter electrode. The working electrodes were made by casting slurry containing active material, carbon black, and PVDF binder with a certain mass ration on a Cu foil. The mass ratios were 8:1:1 and 6.5:2.5:1 for the NTP⊂GN and NTP nanoparticle electrodes, respectively. Note that all the capacity values for the NTP⊂GN electrodes were calculated based on the mass of NTP, which was 65% of the whole electrodes including NTP, graphene, carbon black, and PVDF. The electrodes were dried at 80 °C for 12 h, and then assembled into the coin cells in a glove filled with argon. The diameter of working electrode was 10 mm. The mass loading of active materials was about 1.5 mg cm^{-2}, and the film thickness was about 20 μm. The electrolyte was composed of 1 M NaClO$_4$ in the ethylene carbonate/diethyl carbonate (1:1 v/v) and 5 wt % fluoroethylene carbonate (FEC) additive. The galvanostatic charge−discharge tests were performed on a battery system (Neware BTS) within a cutoff voltage range from 1.5 to 3 V. The specific capacity was calculated based on the mass of active materials. Cyclic voltammetry measurements were carried out by an electrochemical workstation (VoltaLab 80) at a scanning rate of 0.2 mV s^{-1}.

Conflict of Interest: The authors declare no competing financial interest.

Supporting Information Available: Additional XRD patterns and SEM images of NTP⊂GN, the cyclic voltammetry data of the NTP particle electrode, and the HRTEM images and electrochemical impedance spectra of the NTP⊂GN and NTP particle electrodes. The Supporting Information is available free of charge on the ACS Publications website at DOI: 10.1021/acsnano.5b02787.

REFERENCES AND NOTES

1. Armand, M.; Tarascon, J. M. Building Better Batteries. *Nature* **2008**, *451*, 652–657.
2. Tarascon, J. M. Is Lithium the New Gold? *Nat. Chem.* **2010**, *2*, 510–510.
3. Ong, S. P.; Chevrier, V. L.; Hautier, G.; Jain, A.; Moore, C.; Kim, S.; Ma, X.; Ceder, G. Voltage, Stability and Diffusion Barrier Differences Between Sodium-Ion and Lithium-Ion Intercalation Materials. *Energy Environ. Sci.* **2011**, *4*, 3680–3688.
4. Yang, Z.; Zhang, J.; Kintner-Meyer, M. C. W.; Lu, X.; Choi, D.; Lemmon, J. P.; Liu, J. Electrochemical Energy Storage for Green Grid. *Chem. Rev.* **2011**, *111*, 3577–3613.
5. Li, Z.; Young, D.; Xiang, K.; Carter, W. C.; Chiang, Y. M. Towards High Power High Energy Aqueous Sodium-Ion Batteries: The $NaTi_2(PO_4)_3/Na_{0.44}MnO_2$ System. *Adv. Energy Mater.* **2013**, *3*, 290–294.
6. Delmas, C.; Cherkaoui, F.; Nadiri, A.; Hagenmuller, P. A NASICON-Type Phase as Intercalation Electrode-$NaTi_2$-$(PO4)_3$. *Mater. Res. Bull.* **1987**, *22*, 631–639.
7. Wu, X.; Sun, M.; Shen, Y.; Qian, J.; Cao, Y.; Ai, X.; Yang, H. Energetic Aqueous Rechargeable Sodium-Ion Battery Based on $Na_2CuFe(CN)_6$-$NaTi_2(PO_4)_3$ Intercalation Chemistry. *ChemSusChem* **2014**, *7*, 407–411.
8. Li, X.; Zhu, X.; Liang, J.; Hou, Z.; Wang, Y.; Lin, N.; Zhu, Y.; Qian, Y. Graphene-Supported $NaTi_2(PO4)_3$ as a High Rate Anode Material for Aqueous Sodium Ion Batteries. *J. Electrochem. Soc.* **2014**, *161*, A1181–A1187.
9. Wu, W.; Mohamed, A.; Whitacre, J. F. Microwave Synthesized $NaTi_2(PO_4)_3$ as an Aqueous Sodium-Ion Negative Electrode. *J. Electrochem. Soc.* **2013**, *160*, A497–A504.
10. Pang, G.; Nie, P.; Yuan, C.; Shen, L.; Zhang, X.; Li, H.; Zhang, C. Mesoporous $NaTi_2(PO_4)_3$/CMK-3 Nanohybrid as Anode for Long-Life Na-Ion Batteries. *J. Mater. Chem. A* **2014**, *2*, 20659–20666.
11. Hou, Z.; Li, X.; Liang, J.; Zhu, Y.; Qian, Y. An Aqueous Rechargeable Sodium Ion Battery Based on a $NaMnO_2$-$NaTi_2(PO_4)_3$ Hybrid System for Stationary Energy Storage. *J. Mater. Chem. A* **2015**, *3*, 1400–1404.
12. Pang, G.; Yuan, C.; Nie, P.; Ding, B.; Zhu, J.; Zhang, X. Synthesis of NASICON-Type Structured $NaTi_2(PO_4)_3$-Graphene Nanocomposite as an Anode for Aqueous Rechargeable Na-Ion Batteries. *Nanoscale* **2014**, *6*, 6328–6334.
13. Li, W. J.; Chou, S. L.; Wang, J. Z.; Liu, H. K.; Dou, S. X. A New, Cheap, and Productive FeP Anode Material for Sodium-Ion Batteries. *Chem. Commun.* **2015**, *51*, 3682–3685.
14. Kim, Y.; Ha, K. H.; Oh, S. M.; Lee, K. T. High-Capacity Anode Materials for Sodium-Ion Batteries. *Chem.—Eur. J.* **2014**, *20*, 11980–11992.
15. Palomares, V.; Casas-Cabanas, M.; Castillo-Martinez, E.; Han, M. H.; Rojo, T. Update on Na-Based Battery Materials. A Growing Research Path. *Energy Environ. Sci.* **2013**, *6*, 2312–2337.
16. Komaba, S.; Murata, W.; Ishikawa, T.; Yabuuchi, N.; Ozeki, T.; Nakayama, T.; Ogata, A.; Gotoh, K.; Fujiwara, K. Electrochemical Na Insertion and Solid Electrolyte Interphase for Hard-Carbon Electrodes and Application to Na-Ion Batteries. *Adv. Funct. Mater.* **2011**, *21*, 3859–3867.
17. Senguttuvan, P.; Rousse, G.; Seznec, V.; Tarascon, J. M.; Palacin, M. R. $Na_2Ti_3O_7$: Lowest Voltage Ever Reported Oxide Insertion Electrode for Sodium Ion Batteries. *Chem. Mater.* **2011**, *23*, 4109–4111.
18. Li, W. J.; Chou, S. L.; Wang, J. Z.; Liu, H. K.; Dou, S. X. Simply Mixed Commercial Red Phosphorus and Carbon Nanotube Composite with Exceptionally Reversible Sodium-Ion Storage. *Nano Lett.* **2013**, *13*, 5480–5484.
19. Zhu, H. L.; Jia, Z.; Chen, Y. C.; Weadock, N.; Wan, J. Y.; Vaaland, O.; Han, X. G.; Li, T.; Hu, L. B. Tin Anode for Sodium-Ion Batteries Using Natural Wood Fiber as a Mechanical Buffer and Electrolyte Reservoir. *Nano Lett.* **2013**, *13*, 3093–3100.
20. Liu, J.; Wen, Y. R.; van Aken, P. A.; Maier, J.; Yu, Y. Facile Synthesis of Highly Porous Ni-Sn Intermetallic Microcages with Excellent Electrochemical Performance for Lithium and Sodium Storage. *Nano Lett.* **2014**, *14*, 6387–6392.
21. Darwiche, A.; Marino, C.; Sougrati, M. T.; Fraisse, B.; Stievano, L.; Monconduit, L. Better Cycling Performances of Bulk Sb in Na-Ion Batteries Compared to Li-Ion Systems: An Unexpected Electrochemical Mechanism. *J. Am. Chem. Soc.* **2012**, *134*, 20805–20811.
22. Wu, L.; Hu, X. H.; Qian, J. F.; Pei, F.; Wu, F. Y.; Mao, R. J.; Ai, X. P.; Yang, H. X.; Cao, Y. L. Sb-C Nanofibers with Long Cycle Life as an Anode Material for High-Performance Sodium-Ion Batteries. *Energy Environ. Sci.* **2014**, *7*, 323–328.
23. Qian, J. F.; Xiong, Y.; Cao, Y. L.; Ai, X. P.; Yang, H. X. Synergistic Na-Storage Reactions in Sn_4P_3 as a High-Capacity, Cycle-Stable Anode of Na-Ion Batteries. *Nano Lett.* **2014**, *14*, 1865–1869.
24. Qu, B. H.; Ma, C. Z.; Ji, G.; Xu, C. H.; Xu, J.; Meng, Y. S.; Wang, T. H.; Lee, J. Y. Layered SnS_2-Reduced Graphene Oxide Composite—A High-Capacity, High-Rate, and Long-Cycle Life Sodium-Ion Battery Anode Material. *Adv. Mater.* **2014**, *26*, 3854–3859.
25. Zhou, X.; Zhu, X.; Liu, X.; Xu, Y.; Liu, Y.; Dai, Z.; Bao, J. Ultralong Cycle Life Sodium-Ion Battery Anodes Using a Graphene-Templated Carbon Hybrid. *J. Phys. Chem. C* **2014**, *118*, 22426–22431.
26. Zhu, C.; Song, K.; van Aken, P. A.; Maier, J.; Yu, Y. Carbon-Coated $Na_3V_2(PO_4)_3$ Embedded in Porous Carbon Matrix: An Ultrafast Na-Storage Cathode with the Potential of Outperforming Li Cathodes. *Nano Lett.* **2014**, *14*, 2175–2180.
27. Aravindan, V.; Ling, W. C.; Hartung, S.; Bucher, N.; Madhavi, S. Carbon-Coated $LiTi_2(PO_4)_3$: An Ideal Insertion Host for Lithium-Ion and Sodium-Ion Batteries. *Chem.—Asian J.* **2014**, *9*, 878–882.
28. Wu, X.; Cao, Y.; Ai, X.; Qian, J.; Yang, H. A Low-Cost and Environmentally Benign Aqueous Rechargeable Sodium-Ion Battery Based on $NaTi_2(PO_4)_3$-$Na_2NiFe(CN)_6$ Intercalation Chemistry. *Electrochem. Commun.* **2013**, *31*, 145–148.
29. Il Park, S.; Gocheva, I.; Okada, S.; Yamaki, J. Electrochemical Properties of $NaTi_2(PO_4)_3$ Anode for Rechargeable Aqueous Sodium-Ion Batteries. *J. Electrochem. Soc.* **2011**, *158*, A1067–A1070.
30. Wu, W.; Yan, J.; Wise, A.; Rutt, A.; Whitacre, J. F. Using Intimate Carbon To Enhance the Performance of $NaTi_2$-$(PO_4)_3$ Anode Materials: Carbon Nanotubes *vs* Graphite *J. Electrochem. Soc.* **2014**, *161*, A561–A567.
31. Kudin, K. N.; Ozbas, B.; Schniepp, H. C.; Prud'homme, R. K.; Aksay, I. A.; Car, R. Raman Spectra of Graphite Oxide and Functionalized Graphene Sheets. *Nano Lett.* **2008**, *8*, 36–41.
32. Kosynkin, D. V.; Higginbotham, A. L.; Sinitskii, A.; Lomeda, J. R.; Dimiev, A.; Price, B. K.; Tour, J. M. Longitudinal Unzipping of Carbon Nanotubes To Form Graphene Nanoribbons. *Nature* **2009**, *458*, 872–876.
33. Li, S.; Dong, Y.; Xu, L.; Xu, X.; He, L.; Mai, L. Effect of Carbon Matrix Dimensions on the Electrochemical Properties of $Na_3V_2(PO_4)_3$ Nanograins for High-Performance Symmetric Sodium-Ion Batteries. *Adv. Mater.* **2014**, *26*, 3545–3553.
34. Liu, Y.; Xu, Y.; Zhu, Y.; Culver, J. N.; Lundgren, C. A.; Xu, K.; Wang, C. Tin-Coated Viral Nanoforests as Sodium-Ion Battery Anodes. *ACS Nano* **2013**, *7*, 3627–3634.
35. Xu, Y.; Zhu, Y.; Liu, Y.; Wang, C. Electrochemical Performance of Porous Carbon/Tin Composite Anodes for Sodium-Ion and Lithium-Ion Batteries. *Adv. Energy Mater.* **2013**, *3*, 128–133.
36. Chihara, K.; Kitajou, A.; Gocheva, I. D.; Okada, S.; Yamaki, J. Cathode Properties of $Na_3M_2(PO_4)_2F_3$ M = Ti, Fe, V for Sodium-Ion Batteries. *J. Power Sources* **2013**, *227*, 80–85.
37. Nose, M.; Shiotani, S.; Nakayama, H.; Nobuhara, K.; Nakanishi, S.; Iba, H. $Na_4Co_{2.4}Mn_{0.3}Ni_{0.3}(PO_4)_2P_2O_7$: High Potential and High Capacity Electrode Material for Sodium-Ion Batteries. *Electrochem. Commun.* **2013**, *34*, 266–269.